

Study of turbulent fluctuations driven by the electron temperature gradient in the National Spherical Torus Experiment

E. Mazzucato,^{1,*} R. E. Bell,¹ S. Ethier,¹ J. C. Hosea,¹ S. M. Kaye,¹ B. P. LeBlanc,¹ W. W. Lee,¹ P. M. Ryan,² D. R. Smith,¹ W. X. Wang,¹ J. R. Wilson,¹ H. Yuh³

¹Princeton Plasma Physics Laboratory, Princeton University, Princeton, New Jersey 08543, USA

²Oak Ridge National Laboratory, Oak Ridge, Tennessee 37831, USA

³Nova Photonics Inc., Princeton, NJ 08540, USA

*E-mail: mazzucato@pppl.gov

Abstract

Various theories and numerical simulations support the conjecture that the ubiquitous problem of anomalous electron transport in tokamaks may arise from a short-scale turbulence driven by the electron temperature gradient. To check whether this turbulence is present in plasmas of the National Spherical Torus Experiment (NSTX), measurements of turbulent fluctuations were performed with coherent scattering of electromagnetic waves. Results from plasmas heated by high harmonic fast waves (HHFW) show the existence of density fluctuations in the range of wave numbers $k_{\perp}\rho_e=0.1-0.4$, corresponding to a turbulence scale length of the order of the collisionless skin depth. Experimental observations and agreement with numerical results from a linear gyro-kinetic stability code indicate that the observed turbulence is driven by the electron temperature gradient. These turbulent fluctuations were not observed at the location of an internal transport barrier driven by a negative magnetic shear.

PACS numbers: 52.55.Fa, 52.35.Qz, 52.35.Ra

1. Introduction

Understanding the mechanism of plasma transport in tokamaks is one of the great challenges of fusion research. Indeed, since most explanations of this phenomenon are based on some type of turbulence [1-3], understanding plasma transport depends upon understanding turbulence. Unfortunately, since this is a tremendously difficult problem, the cause of anomalous energy losses in tokamaks is still an outstanding issue.

Particularly difficult to explain is the transport of electron energy. This is the most worrisome since in a tokamak reactor a large fraction of the energy of charged fusion products – necessary to sustain the nuclear fusion reactions – would be released directly to the electrons. Various theories and numerical simulations [4–9] support the conjecture that anomalous electron transport may arise from a turbulence driven by the Electron Temperature Gradient (ETG) instability. However, even though a limited circumstantial evidence has been presented in [10] on the role of an ETG turbulence on electron transport in Tore Supra, and measurements on FT-2 of fluctuations with an electron gyro-scale have been reported in [11], the existence of a turbulence driven by the electron temperature gradient in tokamaks has never been proven experimentally.

To investigate this type of turbulence, a series of experiments have been performed in plasmas of the National Spherical Torus Experiment (NSTX). These plasmas are uniquely suited for the

study of the physics of electron transport since, while the confinement of ions in NSTX is very often at or near neoclassical levels, that of electrons is anomalous in all operational regimes [12]. Preliminary results from these experiments have been presented in [13]. Here, we give a more detailed description of measurements of short scale turbulent fluctuations driven by the electron temperature gradient in NSTX plasmas.

2. Coherent scattering of electromagnetic waves

Short-scale density fluctuations were measured with coherent scattering of electromagnetic waves, a powerful technique that was used extensively in early studies of plasma turbulence, including the first detection of short-scale turbulent fluctuations in tokamaks [14]. The process can be characterized by an effective differential cross section per unit volume

$$\sigma = r_0^2 S(\mathbf{k}, \omega), \quad (1)$$

where $r_0 = e^2/mc^2$ is the classical radius of electrons and $S(\mathbf{k}, \omega)$ is the spectral density of fluctuations [15]. The mean square density fluctuation is obtained from

$$\langle |\tilde{n}_e|^2 \rangle = \frac{1}{(2\pi)^4} \int S(\mathbf{k}, \omega) d\mathbf{k} d\omega. \quad (2)$$

Frequency (ω) and wave vector (\mathbf{k}) of fluctuations must satisfy the energy and momentum conservation

$$\omega = \omega_s - \omega_i, \quad \mathbf{k} = \mathbf{k}_s - \mathbf{k}_i, \quad (3)$$

where the superscripts s and i refer to scattered and incident waves, respectively. Since for the topic of this paper $\omega_s \approx \omega_i$ and $k_s \approx k_i$, the scattering angle θ must satisfy the Bragg condition $k = 2k_i \sin(\theta/2)$.

The NSTX scattering system (figure 1) employs a probing wave with a frequency of 280 GHz, together with a five-channel heterodyne receiver capable of providing full information on the frequency spectrum of measured signals [16]. The unique feature of the scattering geometry is the oblique propagation of the probing beam with respect to the magnetic field, with both probe and scattered waves lying nearly on the equatorial midplane (figure 2). Consequently, the wave vectors of measured fluctuations are almost perpendicular to the magnetic sur-

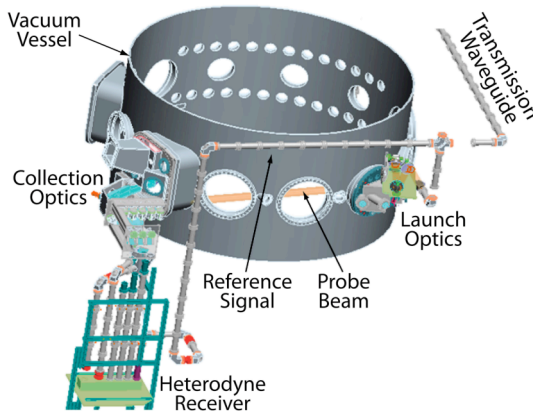


Figure 1. Arrangement of main hardware components of the NSTX scattering system.

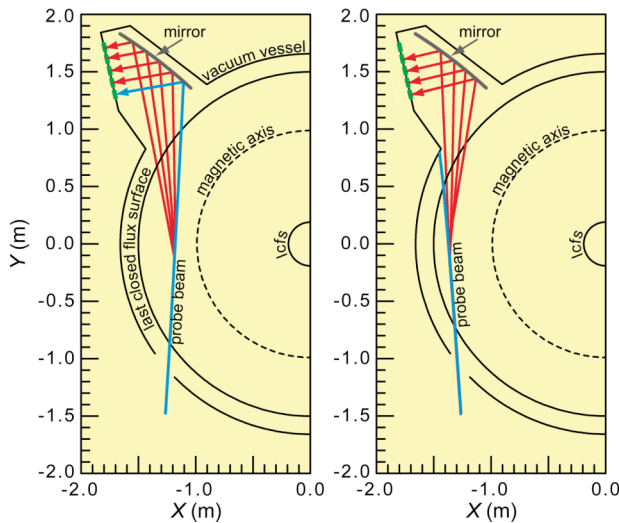


Figure 2. Probe beam (blue) and scattered waves (red) for detection of inboard (left) and outboard (right) fluctuations. Steerable optics can position the scattering region from the magnetic axis to the plasma edge.

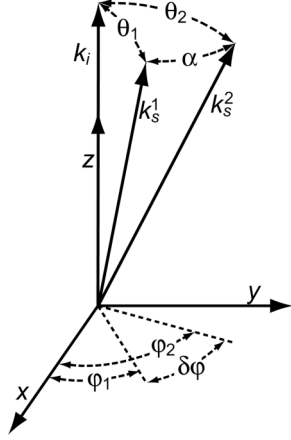


Figure 3. Orthogonal coordinates (x,y,z) with the z -axis along the wave vector of probing beam.

faces. However, they also have small components in both diamagnetic and toroidal directions from which one can infer the phase velocity of fluctuations.

The instrumental resolution of scattering measurements is limited by the size of the probing and scattered beams, both having a Gaussian profile with a radius (a) of 2.5 cm in the present experiment. If we take the size of the region that the two beams have in common as a measure of spatial resolution (δl), we get $\delta l = 4k_i a / k$, that in our case gives $\delta l = 60$ cm for $k = 10$ cm⁻¹. From this, we might conclude that it is difficult to perform localized measurements of plasma turbulence with

coherent scattering of electromagnetic waves. Fortunately, this estimate is valid only for an isotropic turbulence, which is not the case of tokamak plasmas where short-scale fluctuations satisfy the relation $\mathbf{k} \cdot \mathbf{B} / B \approx 1/qR$ [1,2] (with \mathbf{B} the magnetic field, q the magnetic safety factor and R the plasma major radius). For all practical purposes, then, we can assume

$$\mathbf{k} \cdot \mathbf{B} = 0, \quad (4)$$

which, because of the large curvature of magnetic field lines, makes the instrumental selectivity function, i.e., the collection efficiency of scattered waves, strongly localized [17, 18]. This can be seen by considering scattered waves originating from two points of the probing beam with wave vectors \mathbf{k}_s^1 and \mathbf{k}_s^2 , respectively. From figure 3, we get

$$\frac{\mathbf{k}_s^1 \cdot \mathbf{k}_s^2}{k_i^2} \equiv \cos \alpha = \cos \theta_1 \cos \theta_2 + \sin \theta_1 \sin \theta_2 (\cos \varphi_1 \cos \varphi_2 + \sin \varphi_1 \sin \varphi_2), \quad (5)$$

giving

$$\cos \alpha = \cos(\theta_2 - \theta_1) - 2 \sin \theta_1 \sin \theta_2 \sin^2(\delta\varphi/2) \quad (6)$$

where $\delta\varphi = \varphi_2 - \varphi_1$. Since in the present experiment both scattering angles θ_1 and θ_2 are small, we may write

$$\alpha^2 \approx (\theta_2 - \theta_1)^2 + 4\theta_1\theta_2 \sin^2(\delta\varphi/2). \quad (7)$$

Then, if the receiving antenna is positioned for collecting with maximum efficiency the scattered waves from the first point, those from the second will be collected with the relative efficiency $\exp(-\alpha^2/\alpha_0^2)$, where $\alpha_0 = 2/k_i a$ [17, 18]. From this and equation (7), we obtain the instrumental selectivity function

$$F = \exp\left[-\left((k' - k)^2 + 4k'k \sin^2(\delta\varphi/2)\right)/\Delta^2\right], \quad (8)$$

where $\Delta = 2/a$, $k \approx k_i \theta_1$ is the tuning wave number of the receiving antenna and $k' \approx k_i \theta_2$ is the wave number of detected fluctuations. The contour plot of F as a function of position along the probing beam (s) and the wave number mismatch ($\Delta k = k' - k$) is shown in figure 4, where the value of $\delta\varphi$ is from a ray tracing code using the equilibrium reconstruction code EFIT [19] together with equations (3) and (4). This shows that indeed the length of the scattering region is

substantially smaller than the previous estimate of δl for isotropic turbulence. In addition, because of the novel scattering geometry, the radial footprint of the scattering region is smaller than the diameter of the probing beam ($2a$), so that the radial resolution of our fluctuation measurements is ± 2.5 cm together with a wave number resolution of ± 1 cm⁻¹.

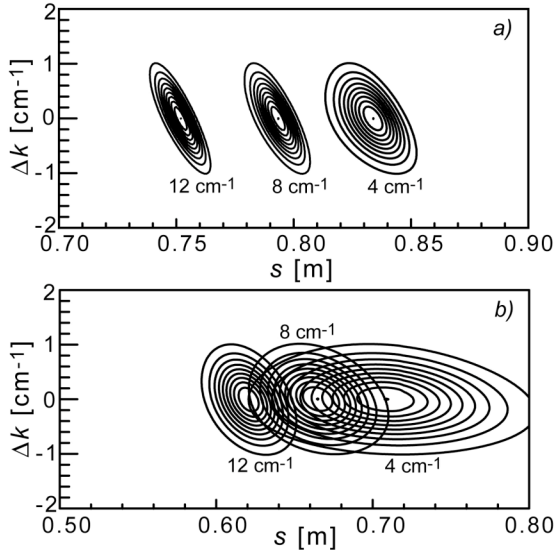


Figure 4. Contour plot of F (ten levels equally spaced from 0.1 to 1, with maximum at $\Delta k=0$) as a function of position along the probe beam (s) and $\Delta k=k'-k$ for the two scattering configurations of figure 2 ((a) inboard fluctuations, (b) outboard fluctuations). Labels are values of k .

by the need to minimize the spurious effects of MHD turbulence. In addition, because of the low plasma density, i.e., a weak electron-ion coupling, the ion temperature (T_i) remained nearly constant (with central values of 0.8-1.0 keV).

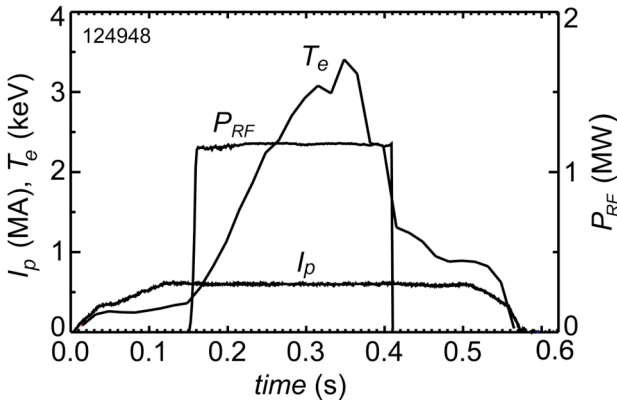


Figure 5. Time evolution of plasma current (I_p), RF power (P_{RF}) and peak electron temperature (T_e).

3. Results

The experimental results presented in this paper were obtained in plasmas with high harmonic fast wave (HHFW) heating [20]. Use of this radio frequency (RF) technique – where a wave having the frequency (30 MHz) of an ion cyclotron harmonic ($\sim 10^{\text{th}}$) is absorbed by the electrons – was motivated by its ability to produce electron temperature (T_e) profiles with large central values and steep gradients. An example is illustrated in figures 5 and 6, showing the case of a Helium discharge with a minor radius of 0.65 m, a major radius of 0.85 m, an elongation of 2, a toroidal magnetic field of 0.55 T, a plasma current of 700 kA and an RF heating power of 1.2 MW. Use of the maximum available magnetic field and of a relatively low plasma current was motivated

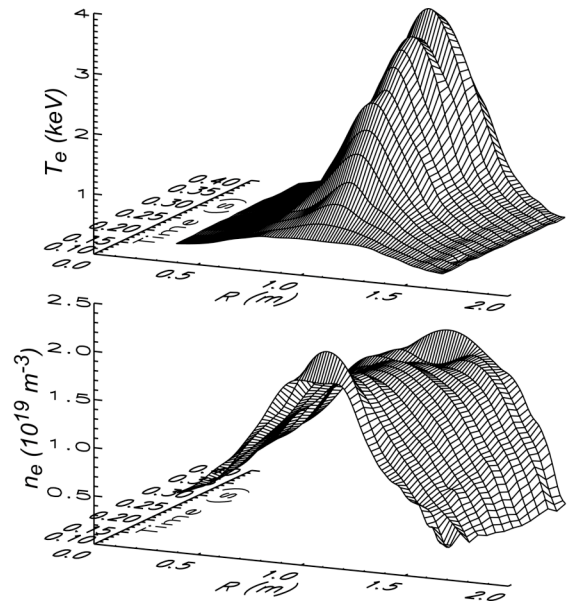


Figure 6. Radial profiles of electron temperature T_e (top) and density n_e (bottom) in plasmas with 1.2 MW of HHFW heating.

Figure 7 shows the time evolution of the spectral density of fluctuations with $k_{\perp}=14\text{ cm}^{-1}$ at $r/a=0.3$ ($R=1.2\text{ m}$), corresponding to the range of $k_{\perp}\rho_e=0.2-0.4$ (with ρ_e the electron gyro-radius), $k_{\perp}\rho_s=8.5-17$ (with ρ_s the ion gyro-radius at the electron temperature) and $k_{\perp}\rho_i=8-10$ (with ρ_i the ion gyro-radius). The latter implies that the source of observed fluctuations is not the Ion Temperature Gradient (ITG) mode, which is instead characterized by $k_{\perp}\rho_i < 1$ [1-3]. This mode is also excluded by the frequency asymmetry of measured spectra, as shown in figure 7, indicating that fluctuations propagate in the electron diamagnetic direction. Finally, the large values of $k_{\perp}\rho_s$ seem to exclude the Trapped Electron Mode (TEM) as well.

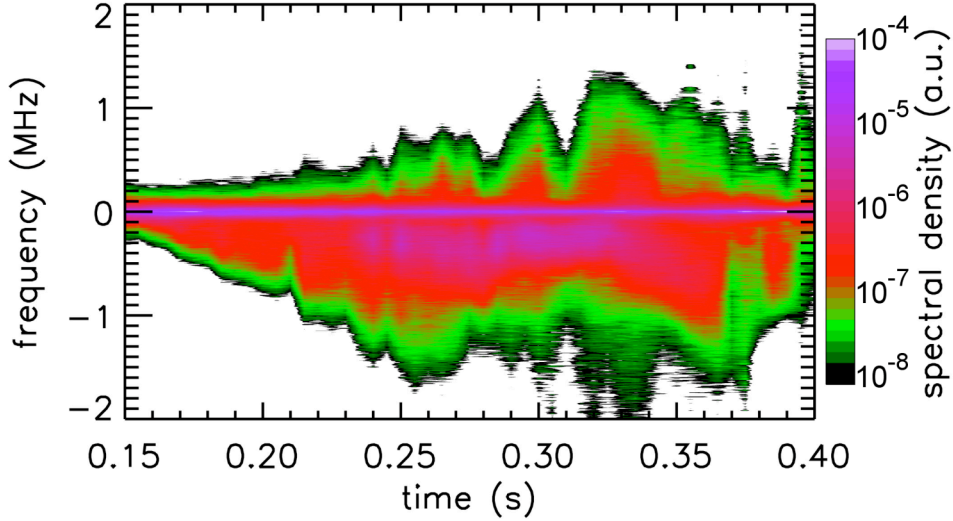


Figure 7. Logarithmic contour plot of the spectral density of fluctuations with $k_{\perp}\rho_e=0.2-0.4$ at $r/a=0.3$. Negative frequencies correspond to a wave propagation in the electron diamagnetic direction.

It is interesting to note that for the plasma density in figure 6, $k_{\perp}\delta_{sk} \sim 2$, where δ_{sk} is the collisionless skin depth ($c/\omega_{pe} = \rho_e/\beta_e^{1/2}$), with ω_{pe} the plasma frequency and β_e the electron beta. This is not surprising since for sufficiently large values of β_e , such as those in the present experiment (3-6%), the characteristic turbulence scale length is expected to be of the order of the collisionless skin depth [4, 21].

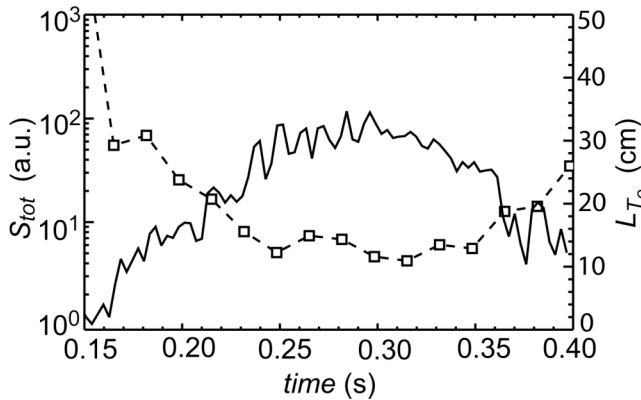


Figure 8. Frequency integrated spectral density S_{tot} (solid line) and radial scale L_{Te} (dash line) for the case of figure 7.

These turbulent fluctuations appear to be related to the electron temperature gradient, as illustrated in figure 8 where the frequency integrated value of the spectral density (S_{tot}) is compared with the electron temperature scale length (defined as $L_{Te}=(d\ln T_e/dr)^{-1}$) at the location of measurement. Note that plasma fluctuations begin to rise at the beginning of the RF pulse, when the value of L_{Te} begins to drop, and decrease towards the end of the pulse when the opposite occurs.

The same phenomenon is illustrated in figure 9, showing the electron temperature profile and the spectrum of measured fluctuations at two different times, the first when the amplitude of fluctuations is maximum (0.3 s), the second 30 ms after the RF pulse (0.43 s) when the profile of T_e has collapsed and flattened over a wide central region. At the location of measurement (blue stripe in figure 9), both ion and electron temperatures and plasma densities are the same in both cases, while the values of L_{T_e} differ by a factor of three (15 vs 50 cm). Correspondingly, while both spectra contain a central narrow symmetric feature – caused by spurious stray radiation – that at 0.3 s displays a strong Doppler shifted component, which is that of scattering signals from large plasma fluctuations. These results clearly demonstrates the dependence of measured turbulence on the radial scale of T_e .

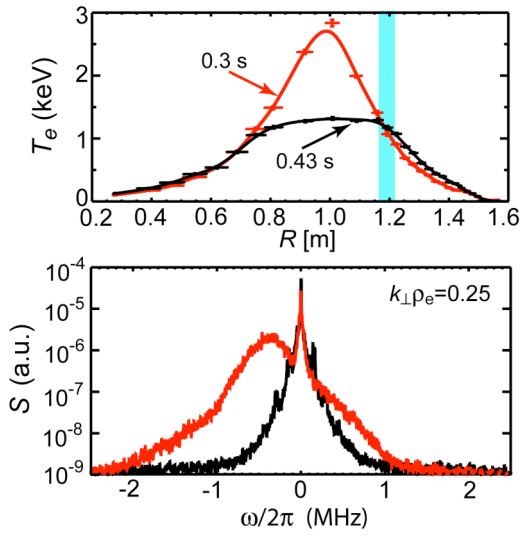


Figure 9. Temperature profiles (top) and spectral density of fluctuations (bottom) at 0.3 s (red) and 0.43 s (black). Blue stripe indicates the location of measurement where L_{T_e} is 15 and 50 cm, respectively. Negative frequencies (bottom) correspond to a wave propagation in the electron diamagnetic direction.

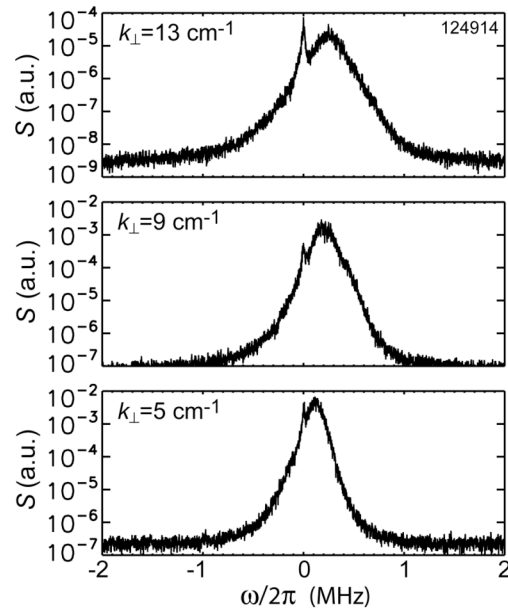


Figure 10. Spectral density of fluctuations in the range of wave numbers $k_{\perp}\rho_e=0.1-0.2$ at $r/a=0.6$. Positive frequencies correspond to a wave propagation in the electron diamagnetic direction.

Short scale turbulent fluctuations were also detected on the outer region of the plasma column ($r/a=0.6$), as illustrated in figure 10 showing the spectral density of fluctuations with wave numbers in the range $k_{\perp}\rho_e=0.1-0.2$ and $k_{\perp}\rho_i \approx k_{\perp}\rho_s = 4-8$. Again, the scale length is of the order of the collisionless skin depth ($k_{\perp}\delta_{sk}=1-2$). As in the case of core fluctuations, wave numbers are outside the range of both ITG and TEM modes, and wave propagation is in the electron diamagnetic direction (corresponding to positive frequencies for the scattering geometry used for these measurements).

The propagation of fluctuations along the electron diamagnetic direction is of crucial importance since it rules out the ITG instability as the source of turbulence. So far in the present paper, the phase propagation of fluctuations was inferred from the sign of measured frequencies when the Doppler shift from a toroidal plasma rotation was negligible, i.e., from the sign of $\omega_s - \omega_i$ together with the component of the wave vector of fluctuations in the diamagnetic direction. Indeed,

the Doppler shift from a plasma rotation could provide further information on the direction of wave propagation. This can be seen by using the orthogonal system of coordinates (θ, φ, ψ) of figure 11, where the unit vector \mathbf{e}_ψ is in the outward normal direction to the magnetic surface (i.e., $\nabla p \cdot \mathbf{e}_\psi < 0$), and \mathbf{e}_φ is parallel to the toroidal plasma current (i.e., $B_\theta > 0$). For short, let us refer to fluctuations that in the plasma frame propagate along the electron diamagnetic velocity ($\mathbf{v}_{De} = \nabla p_e \times \mathbf{B} / en_e B^2$) as electron waves, and those propagating along the ion diamagnetic velocity ($\mathbf{v}_{Di} = -\nabla p_i \times \mathbf{B} / en_i B^2$) as ion waves. From equation (4) – implying that the magnetic surface component of the wave vector of measured fluctuations is in the diamagnetic direction – and from

$$\mathbf{v}_{De} \cdot \mathbf{e}_\varphi = -\frac{|\nabla p_e| B_\theta}{en_e B^2} < 0 \quad (9)$$

and

$$\mathbf{v}_{Di} \cdot \mathbf{e}_\varphi = \frac{|\nabla p_i| B_\theta}{en_e B^2} > 0, \quad (10)$$

we conclude that a plasma co-rotation (i.e., in the plasma current direction) produces a Doppler shift in the frequency of scattered signals by electron waves with the opposite sign of the

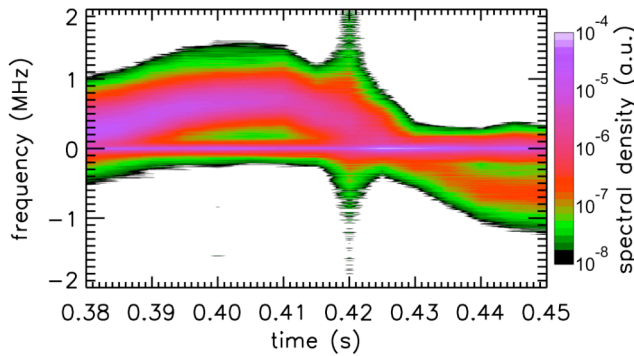


Figure 12. Time evolution of the spectrum of fluctuations with $k_\perp = 13 \text{ cm}^{-1}$ for the plasma rotation of figure 13 (burst at 0.42 s was caused by the abrupt termination of the RF pulse by the onset of an MHD instability).

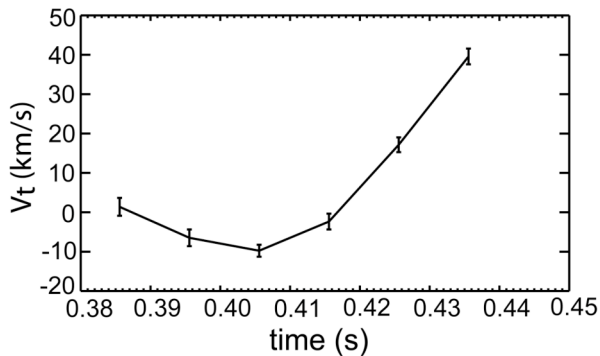


Figure 13. Time evolution of toroidal plasma velocity v_t (positive when along the plasma current).

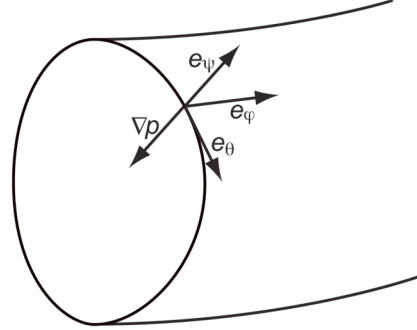


Figure 11. Orthogonal coordinate system (θ, φ, ψ) with \mathbf{e}_ψ along the outward normal to the magnetic surface and \mathbf{e}_φ parallel to the toroidal plasma current.

frequency itself when measured in the plasma frame (i.e., in the absence of plasma rotation), and the contrary for ion waves. A plasma counter-rotation has the opposite effect, i.e., a frequency Doppler shift in the frequency of scattered signals by electron waves with the same sign of the frequency itself when measured in the plasma frame, and the contrary for ion waves. Figures 12 and 13, which display the time evolution of the spectrum of fluctuations and of the plasma toroidal velocity v_t (driven in part by the neutral beam used for velocity measurements with the method of charge exchange recombination spectroscopy), demonstrate that the frequency follows the toroidal velocity as just described for the case of electron waves, while it disagrees completely with what to expect from ion waves, since in this case the measured frequency – that in figure 12 is positive when $v_t = 0$ – should decrease when $v_t < 0$ and

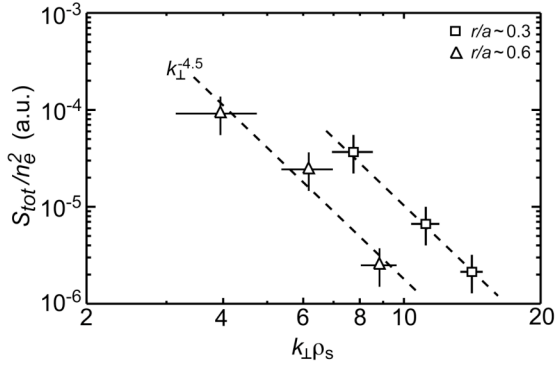


Figure 14. Power spectrum of fluctuations (normalized to the square of local density) as a function of $k_{\perp}\rho_s$ for both inboard (squares) and outboard (triangles) measurements.

would follow the power law $\langle |\tilde{n}_e^2| \rangle / n_e^2 \propto k_{\perp}^{-3.5}$.

5. Negative Magnetic Shear

It is known that a negative magnetic shear can induce – under certain conditions – the formation of internal transport barriers (ITB), resulting in drastically reduced outflow of plasma energy. The signature of an electron ITB is a sharp temperature gradient at the barrier location, inside which the profile of T_e is nearly flat. If the turbulent fluctuations described in this paper are responsible – even if partially – for the electron anomalous transport in tokamaks, they should be suppressed at the location of an electron ITB.

A simple procedure for producing plasmas with negative magnetic shear in NSTX is to launch a high power HHFW pulse during the early phase of a discharge, when the toroidal current is still diffusing from the plasma edge to the center. An example is shown in figure 15, where 3 MW of HHFW were launched into a Deuterium plasma. A strong electron heating together with a low value of Z_{eff} (~ 1.4) had the effect of slowing down the diffusion of plasma current and forming a central region with strong negative magnetic shear (figure 16), which lasted until the onset

increase when $v_t > 0$. Hence the conclusion that measured fluctuations propagate in the electron diamagnetic direction.

Finally, the power spectrum of fluctuations (i.e., the value of S_{tot} normalized to n_e^2) is displayed in figure 14 as a function of $k_{\perp}\rho_s$ for both inboard (figure 7) and outboard (figure 10) measurements. Surprisingly, the power spectrum follows a similar power law ($\sim k_{\perp}^{-4.5}$) at both plasma locations in spite of different electron temperatures (1.5 vs. 0.5 keV). If the measured fluctuations were isotropic perpendicularly to the magnetic field – impossible to prove with our measurements – the mean square density fluctuation

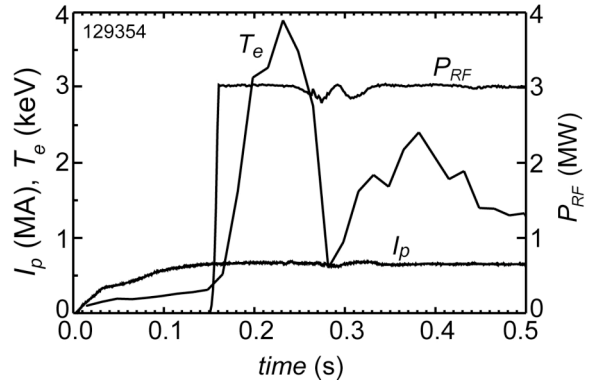


Figure 15. Time evolution of plasma current (I_p), RF power (P_{RF}) and peak electron temperature (T_e) in a plasma with negative magnetic shear.

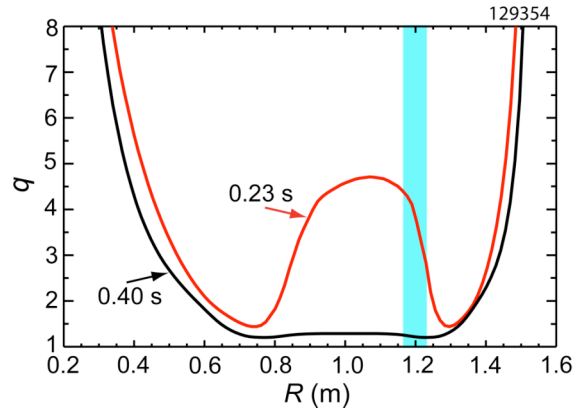


Figure 16. Magnetic safety factor on the equatorial plane at the peak of T_e (red) and after the collapse of negative magnetic shear (black). Blue stripe indicates the location of fluctuation measurements.

of an MHD instability caused a fast redistribution of the plasma current and a flattening of its radial profile. During the phase of negative shear, the electron temperature developed a steep gradient near the radius of minimum q (figure 17), which indicates the presence of an internal transport barrier (ITB) [22]. Figures 18 and 19 show that indeed fluctuations were suppressed at the transport barrier – a striking similarity to what was found previously in similar TFTR plasmas [23], albeit for fluctuations driven by the ion temperature gradient (ITG). However, turbulent fluctuations reappeared (figures 19) as soon as the plasma current diffused to the plasma core, making the q -profile nearly constant over a wide central region (figure 16).

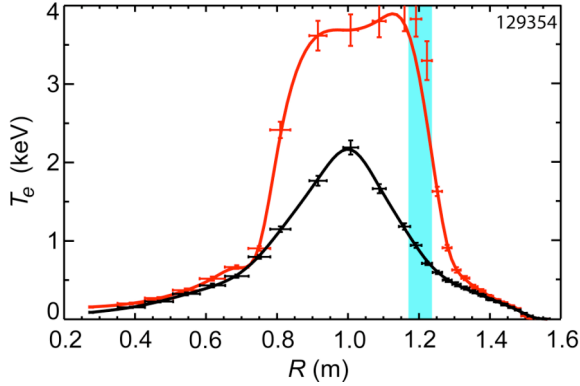


Figure 17. Same as in figure 16 for T_e .

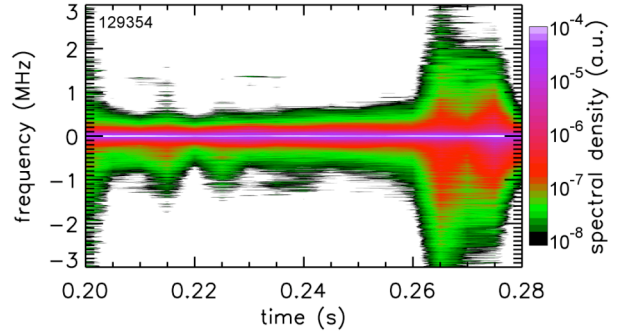


Figure 18. Spectral density of measured fluctuations (with the same scattering geometry of figure 7) during a negative reversed shear. The sudden rise at $t=0.26$ coincides with the collapse of the ITB.

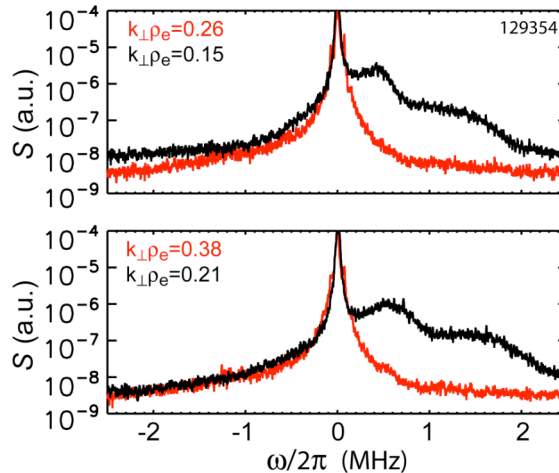


Figure 19. Same as in figure 16 for the spectrum of fluctuations.

4. Discussion

In an attempt to determine the source of observed fluctuations, we employed a linear version of the GS2 stability code [24] to obtain the normalized critical gradient $(R/L_{T_e})_{crit}$ for the onset of the ETG instability. This code solves the gyro-kinetic Vlasov-Maxwell equations, including passing and trapped particles, electromagnetic effects, as well as a Lorentz collision operator. The

results are shown in figure 15, where the critical gradient is compared with the measured normalized temperature gradient R/L_{T_e} for the case of figure 7. From this, we conclude that the ETG mode is indeed unstable over most of the RF pulse where the critical gradient is smaller than the electron temperature gradient. A comparison with S_{tot} in figure 8 shows that the level of measured fluctuations correlates with the departure of the temperature gradient from the critical gradient.

Figure 20 displays also an algebraic expression of the normalized critical gradient that was derived in [25] using a best fit of GS2 results for a set of model tokamak configurations. This is given by

$$(R/L_{T_e})_{crit} = (1 + Z_{eff} T_e/T_i)(1.3 + 1.9s/q)(1 - 1.5\varepsilon), \quad (11)$$

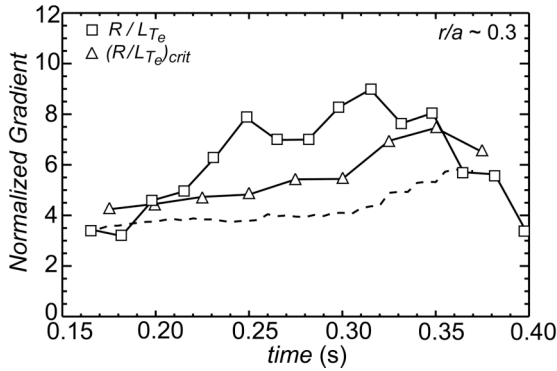


Figure 20. Time evolution of measured gradient R/L_{T_e} (squares) and GS2 critical gradient $(R/L_{T_e})_{crit}$ (triangles) for the onset of the ETG mode in case of figure 7. Dash line is the critical gradient from [25].

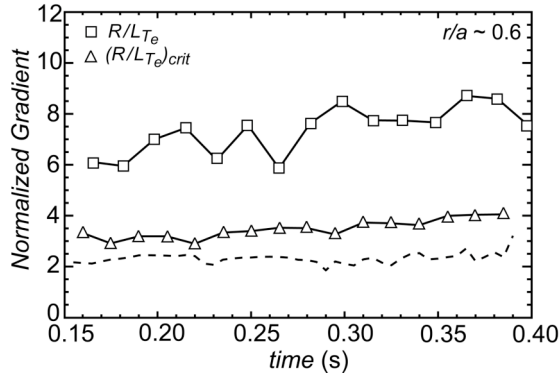


Figure 21. Same as in figure 20 for the case of figure 10.

The observed fluctuations were also compared with numerical results of a nonlinear simulation of short-scale plasma turbulence using the Gyro-kinetic Tokamak Simulation code (GTS) [26] – a numerical tool capable of

where Z_{eff} is the ionic effective charge (~ 2.5 in figure 20), $s = r(d \ln q / dr)$ is the magnetic shear and $\varepsilon = r/R$ is the inverse aspect ratio. This formula, showing the stabilizing role of Z_{eff} , the temperature ratio T_e/T_i and the magnetic shear, gives values of critical gradient that are not very different from those obtained from the GS2 code using the exact equilibrium configuration of our plasmas.

Similar plots are displayed in figure 21 for the case of outboard fluctuations (figure 10), showing again that fluctuations coincide with a temperature gradient larger than the critical gradient. At this plasma location, however, since the HHFW heating did not modify significantly plasma conditions, both the amplitude of measured fluctuations and the ETG critical gradient remained nearly constant in time.

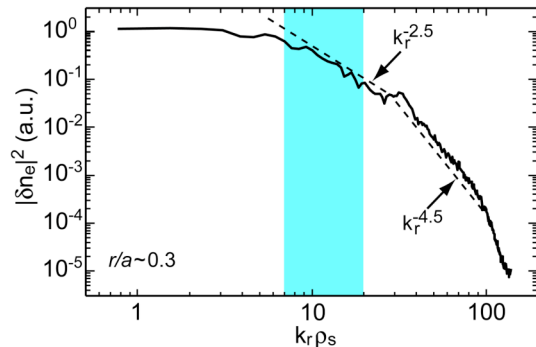


Figure 22. Power spectrum of density fluctuations from the GTS code for the case of $r/a=0.3$ in figure 14 (blue stripe indicates the range of wave numbers of measured fluctuations).

providing a global picture of electrostatic turbulence in realistic tokamak configurations. Because of the extremely high resolution required for electron-scale fluctuations, ions were treated adiabatically, i.e., neglecting the coupling to ion-scale fluctuations. This is not a serious problem in NSTX plasmas, where turbulent fluctuations with low wave numbers are suppressed by a large $E \times B$ velocity shear [12]. More serious is instead the inability of GTS to deal with electromagnetic effects, an extremely difficult problem – if not impossible – for present nonlinear gyro-kinetic simulations of plasma turbulence.

Figure 22 shows the calculated power spectrum of density fluctuations as a function of $k_r \rho_s$ for $r/a=0.3$. It confirms that in the range of measured wave numbers the spectrum follows a power law, albeit with a different exponential power of -2.5. A nonlinearly generated zonal flow was also observed in the simulation during the development of turbulence. However, the zonal flow is significantly weaker than what is found for ITG turbulence, indicating that radial elongated streamers can survive making fluctuations anisotropic perpendicularly to the magnetic field.

5. Conclusion

In conclusion, turbulent fluctuations have been observed in NSTX plasmas in the range of wave numbers $k_{\perp} \rho_e = 0.1-0.4$, corresponding to a radial scale of the order of the collisionless skin depth. Large values of $k_{\perp} \rho_i$, a strong correlation with the scale of T_e and a phase propagation in the electron diamagnetic direction exclude the ITG mode as the source of turbulence. Similarly, the TEM mode cannot explain our observations because of the large values of $k_{\perp} \rho_s$. Experimental observations and agreement with numerical results from the linear gyro-kinetic GS2 code support the conjecture that the observed turbulence is driven by the electron temperature gradient.

These fluctuations were not observed at the location of an internal transport barrier driven by a strong negative magnetic shear. Even though this could be used as evidence of the role played by measured fluctuations on plasma transport, additional experiments together with nonlinear numerical simulations of plasma turbulence are needed before reaching any definite conclusion on the importance of observed fluctuations.

Acknowledgments

This work was supported by U. S. Department of Energy Contract No. DE-AC02-76CH03073. The authors would like to thank the entire NSTX operations, physics, and engineering teams for their contributions to this effort.

References

- [1] B. Coppi and G. Rewoldt, in *Advances in Plasma Physics*, edited by A. Simon and W. B. Thompson (John Wiley and Sons, New York, 1976), Vol. 6, p. 421.
- [2] W. Horton, *Rev. Mod. Phys.* **71**, 735 (1999).
- [3] J. W. Connor and H. R. Wilson, *Plasma Phys Control. Fusion* **36**, 719 (1994).
- [4] W. Horton, P. Zhu, G. T. Hoang, T. Aniel and X. Garbet, *Phys. Plasmas* **7**, 1494 (2000).
- [5] W. Dorland, F. Jenko, M. Kotschereuther and B. N. Rotgers, *Phys. Rev. Lett.* **85**, 5579 (2000).
- [6] F. Jenko and W. Dorland, *Phys. Rev. Lett.* **89**, 225001 (2002).
- [7] W. M. Nevins, J. Candy, S. Cowley, T. Dannert, A. Dimits, W. Dorland, C. Estrada-Mila, G. W. Hammett, F. Jenko, M. J. Pueschel and D. E. Shumaker, *Phys. Plasmas* **13**, 122306 (2006).
- [8] A. M. Dimits, W. N. Nevins, D. E. Shumaker, G. W. Hammett, T. Dannert, F. Jenko, M. J. Pueschel, W. Dorland, S. C. Cowley, J. N. Leboeuf, T. L. Rhodes, J. Candy and C. Estrada-Mila, *Nucl. Fusion* **47**, 817 (2007).
- [9] R. E. Waltz, J. Candy, and M. Fahey, *Phys. Plasma* **14**, 0561116 (2007).
- [10] W. Horton, G. T. Hoang, C. Bourdelle, X. Garbet, M. Ottaviani and L. Colas, *Phys. Plasmas* **11**, 2600 (2004).
- [11] A. D. Gurchenko, E. Z. Gusakov, A. B. Altukhov, A. Yu. Stepanov, L. A. Esipov, M. Yu. Kantor, D. V. Kouprienko, V. V. Dyachenko and S. I. Lashkul, *Nucl. Fusion* **47**, 245 (2007).
- [12] S. M. Kaye, R.E. Bell, D. Gates, B. P. LeBlanc, F. M. Levinton, J.E. Menard, D. Mueller, G. Rewoldt, S.A. Sabbagh, W. Wang and H. Yuh, *Phys. Rev. Lett.* **98**, 175002 (2007).
- [13] E. Mazzucato, D. R. Smith, R. E. Bell, S. M. Kaye, J. C. Hosea, B. P. LeBlanc, J. R. Wilson, P. M. Ryan, C. W. Domier, N. C. Luhmann, Jr., H. Yuh, W. Lee and H. Park, *Phys. Rev. Lett.* **101**, 075001 (2008).
- [14] E. Mazzucato, *Phys. Rev. Lett.* **36**, 792 (1976).
- [15] M. N. Rosenbluth and N. Rostoker, *Phys. Fluids* **5**, 776 (1962).
- [16] D.R. Smith, E. Mazzucato, W. Lee, H. Park, W. Domier and N. C. Luhmann, Jr., *Rev. Sci. Instrum.* **79**, 123501 (2008).

- [17] E. Mazzucato, *Phys. Plasmas* **10**, 753 (2003).
- [18] E. Mazzucato, *Plasma Phys Control. Fusion* **48**, 1749 (2006).
- [19] L. L. Lao, H. St. John, R. D. Stambaugh, A. G. Kellman and W. Pfeiffer, *Nucl. Fusion* **25**, 1611 (1985).
- [20] J. Hosea, R. E. Bell, B. P. LeBlanc, C. K. Phillips, G. Taylor, E. Valeo, J. R. Wilson, E. F. Jaeger, P. M. Ryan, J. Wilgen, H. Y. Yuh, F. Levinton, S. Sabbagh, K. Tritz, J. Parker, P. T. Bonoli and R. Harvey, *Phys. Plasmas* **15**, 056104 (2008).
- [21] B. Coppi, in *Collective Phenomena in Macroscopic Systems*, edited by G. Bertin (World Scientific, Singapore, 2007).
- [22] H. Y. Yuh, F. M. Levinton, R. E. Bell, J. C. Hosea, S. M. Kaye, B. P. LeBlanc, E. Mazzucato, D. R. Smith, J. L. Peterson, H. K. Park, W. Lee, C. W. Domier, and N. C. Luhmann Jr., to be published in *Phys. Plasmas* (2009).
- [23] E. Mazzucato, S. H. Batha, M. Beer, M. Bell, R. E. Bell, R. V. Budny, C. Bush, T. S. Hahm, G. W. Hammett, F. M. Levinton, R. Nazikian, H. Park, G. Rewoldt, G. L. Schmidt, E. J. Synakowski, W. M. Tang, G. Taylor and M. C. Zarnstorff, *Phys. Rev. Lett.*, **77**, 3145 (1996).
- [24] M. Kotschenreuther, G. Rewoldt, and W. M. Tang, *Comput. Phys. Commun.* **88**, 128 (1995).
- [25] F. Jenko, W. Dorland and G. W. Hammett, *Phys. Plasmas* **8**, 4096 (2001).
- [26] W. X. Wang, Z. Lin, W. M. Tang, W. W. Lee, S. Ethier, J. L. V. Lewandowski, G. Rewoldt, T. S. Hahm and J. Manickam, *Phys. Plasmas* **13**, 092505 (2006).